Arabian Journal of Chemistry (2021) **14**, 103159

King Saud University

Arabian Journal of Chemistry

www.ksu.edu.sa
www.sciencedirect.com

ORIGINAL ARTICLE

Phytochemical profiling and anti-aging activities of *Euphorbia retusa* extract: *In silico* and *in vitro* studies

Abdelbaset M. Elgamal [a], Mohamed A. El Raey [b,*], Ahmed Gaara [c], Mohamed A.O. Abdelfattah [d], Mansour Sobeh [e,*]

[a] *Department of Chemistry of Microbial and Natural Products, National Research Centre, Dokki, Cairo 12622, Egypt*
[b] *Department of Phytochemistry and Plant Systematics, Pharmaceutical Division, National Research Centre, Dokki, Cairo 12622, Egypt*
[c] *Department of Chemistry of Natural Compounds, Pharmaceutical Division, National Research Centre, Dokki, Cairo, Egypt*
[d] *College of Engineering and Technology, American University of the Middle East, Kuwait*
[e] *AgroBioSciences Research Department, Mohammed VI Polytechnic University, Lot 660–Hay MoulayRachid, Ben-Guerir 43150, Morocco*

Received 2 March 2021; accepted 6 April 2021
Available online 16 April 2021

KEYWORDS

Euphorbia retusa;
Anti-aging;
Antioxidant;
Collagenase;
Elastase;
Hyaluronidase;
Tyrosinase

Abstract In this work, the phytochemical profiling of *Euphorbia retusa* aerial parts by HPLC-PDA-MS/MS revealed 21 secondary metabolites including phenolic acids, flavonoids, and their glycoside derivatives. The chemical structures of four isolated compounds (Esculetin, quercetin 3-*O*-*β*-D-glucuronide, kaempferol 3-*O*-*β*-D-glucuronide, and kaempferol 3-*O*-*β*-D-glucoside) were elucidated using mass spectrometry, ^{1}H, and ^{13}C NMR spectroscopy. Among the isolated compounds, kaempferol-3-*O*-glucuronide and esculetin were identified for the first time from the plant. An *in silico* molecular docking study showed the high potential of the identified compounds in the extract to bind to the active sites of four enzymes crucially involved in skin remodeling and aging processes. The *in vitro* assay confirmed the docking results against collagenase, elastase, hyaluronidase, and tyrosinase enzymes respectively. Among the four isolated compounds, kaempferol 3-*O*-

* Corresponding authors.
E-mail addresses: elraiy@gmail.com (M.A. El Raey), mohamed.abdelmoety@aum.edu.kw (M.A.O. Abdelfattah), mansour.sobeh@um6p.ma (M. Sobeh).

Peer review under responsibility of King Saud University.

Production and hosting by Elsevier

https://doi.org/10.1016/j.arabjc.2021.103159

glucoside was the highest active compound against the aforementioned enzymes. Moreover, the extract showed substantial antioxidant activity in DPPH assay. In conclusion, *E. retusa* is a substantial source for bioactive secondary metabolites with potential application in aging.

1. Introduction

Organs of human body including skin, which is the outermost protective cover of our body, are subject to age-related changes. Skin is in direct exposure to the external environment, and thus it is one of the most affected organs by environmental damage, which contributes broadly to its aging process. Skin is made by a multilayered structure composed of an underlying matrix named dermis and a functional epidermis of four closely adherent layers at the outer surface (Eun Lee et al., 2019). The epidermis region is rich in keratinocytes that produce the structural keratin protein and stratify towards the outer surface acting as an external barrier. The dermis, on the other side, is packed with fibroblasts, which secretes various structural components known with their significant reparative and wound healing properties. Moreover, this layer helps regulate both extracellular matrices and interstitial fluid volume (Altyar et al., 2020).

Skin aging includes intrinsic (chronologic) and extrinsic aging (photoaging). The former is a natural process induced mainly by the side products of the metabolic activities in skin cells, of which reactive oxygen species (ROS) are the most deleterious. Extrinsic aging, however, is mediated by many different external environmental factors. Excessive production of ROS results in wrinkle development by aiding the cleavage and the abnormal chain crossing of the fibrous proteins elastin, collagen and the glycosaminoglycan hyaluronic acid in the skin extracellular matrix (ECM) (Matos et al., 2019).

Degradation of the fibrous proteins is mainly mediated by metalloproteinases, which constitute a super family of protease enzymes whose catalytic action involves a metal. The cleavage of hyaluronic acid is done mainly by hyaluronidase enzyme that degrades the polymeric molecule at specific links along the chemical structure. Overproduction of the melanin pigment is another prominent sign for skin aging and is regulated by the enzyme tyrosinase. Targeting such enzymes by chemical inhibitors is a promising strategy in retarding and fighting skin aging, especially if these agents possess an appreciable antioxidant potential (Altyar et al., 2020)

During the current era of globalization and technology, a shift in consumers' preference from the synthetic chemicals to the more natural or ''green'' herbal products is very surprising. This shift is a consequence of the increasing concerns about the adverse effects associated with the chemical products. Both international and local medical authorities worldwide have approved the usage of a huge number of plant-based preparations in managing and curing different ailments (Lee et al., 2020).

Euphorbiaceae family comprises many genera including the genus Euphorbia and about 1000 species. It is renowned for providing plant extracts rich in numerous phenolic metabolites (El Raey et al., 2019). Several biological activities were reported from Euphorbia species including antimicrobial, anti-inflammatory, antitumor, hypolipidemic, hepatoprotective, and antihyperglycemic, in addition to a potential to inhibit HIV infection (Anusuya et al., 2010; Bakr et al., 2012; Ghareeb, T et al., 2018; Kumarappan et al., 2011; Saleem et al., 2019). Moreover, methanolic extracts from the leaves and roots of *E. milli* exhibited strong antioxidant potential in various assays and showed substantial inhibition towards alpha glucosidase enzyme, however the dichloromethane extracts of the same plant parts were reported to exert substantial inhibitory effects against acetylcholinesterase and tyrosinase enzymes. This effect was mainly attributed to the plant's high content of polyphenols and flavonoids (Saleem et al., 2019).

Euphorbia retusa is an annual plant abundant to the Mediterranean region. In traditional medicine, *E. retusa* was used to cure warts, trichiasis, and venomous bites (Sdayria et al., 2018). Several secondary metabolites were identified in *E. retusa* extracts such as flavonols with their glycoside derivatives, ellagic acid, dimethoxy ellagic acid (Ghareeb, T et al., 2018; Saleh, 1985), carotenoids, diterpenes, triterpenes, sterols, fatty alcohols, and essential fatty acids (Haba et al., 2009; Shaaban et al., 2018).

In the present work, we profiled the secondary metabolites from the aerial parts of Euphorbia retusa by a liquid chromatography–mass spectrometry (LC-MS/MS) method and purely isolated four phenolic compounds whose chemical structures were elucidated by nuclear magnetic resonance (^{1}H and ^{13}C NMR) spectroscopy and mass spectrometry data. In silico molecular docking was done to evaluate the potential of the identified extract components to interfere with four crucial enzymes for skin remodeling; namely elastase, hyaluronidase, collagenase and tyrosinase. Additionally, the antioxidant and the *in vitro* inhibitory potential of the extract and the four isolated components against the aforementioned enzymes were evaluated.

2. Materials and methods

2.1. Plant material and extraction

The aerial parts of *E. retusa* were collected from Wadi Elnatron, Egypt in September 2016. The plant material was ground, and 500 g was extracted at ambient temperature (7:3: MeOH:H_2O, 3 × 1 L). The obtained extract was evaporated under vacuum till dryness and freeze dried to yield 60 g. A 30 g portion was suspended in water and partitioned by a sequential fractionation using DCM, ethyl acetate and butanol. The yields were DCM (1.2 g), ethyl acetate (2.5 g) and butanol (12 g) fractions.

2.2. Compound isolation

The butanol fraction was loaded to Sephadex LH-20 column chromatography using 50% ethanol as eluent. The dark absorbing color band under UV lamp was collected and examined by two-dimension paper chromatography using BAW and 15% acetic acid (Osman et al., 2016) to yield five major fractions. Each fraction was applied to repeated Sephadex LH-20 column chromatography to yield 4 secondary metabolites.

2.3. Identification of isolated compounds

2.3.1. Esculetin

^{1}H NMR (400 MHz, DMSO d_6) δ ppm 6.11 (d, J = 9.4 Hz, 1H, H-3), 7.82 (d, J = 9.4 Hz, 1H, H-4), 6.93 (s, 1H, H-5), 6.69 (s, 1H, H-8). ^{13}C NMR (101 MHz, DMSO- d_6): δ 103.11 (C-8), 111.09 (C-8a), 111.79, (C-3), 112.66 (C-5), 143.57 (C-6), 145.02 (C-4), 149.11 (C-4a), 151.35 (C-7), 161.41 (C-2).

2.3.2. Quercetin -3-O- β-D-glucuronide

^{1}H NMR (400 MHz, DMSO d_6) δ ppm 6.18 (brs, 1H, H-6), 6.38 (brs, 1H, H-8), 7.59–7.52 (m, 2H, H-2′ & H-6′), 6.81 (d, J = 8.4 Hz, 1H, H-5′), 5.45 (d, J = 6.9 Hz, 1H, H-1″).

^{13}C NMR (101 MHz, DMSO-D_6) δ ppm 177.74 (C-4), 170.78 (C-6″), 164.87 (C-7), 161.67 (C-5), 156.81(C-2), 156.70 (C-9), 149.16 (C-4′), 145.45 (C-3′), 133.64 (C-3), 122.14 (C-6′), 121.34 (C-1′), 116.74 (C-5′), 115.78 (C-2′), 104.35(C-10), 101.69 (C-1″), 99.33 (C-6), 94.14 (C-8), 76.44 (C-3″), 76.30 (C-5″), 74.32 (C-2″), 71.94 (C-4″).

2.3.3. Kaempferol -3-O-β-D-glucuronide

^{1}H NMR (400 MHz, DMSO d_6) δ ppm 6.10 (brs, 1H, H-6), 6.32 (brs, 1H, H-8), 7.99 (d, J = 8.5 Hz, 2H), 6.83 (d, J = 8.7 Hz, 2H), 5.41 (d, J = 7.0 Hz, 1H, H-1″).

^{13}C NMR (101 MHz, DMSO d_6) δ 177.92 (C-4), 168.55 (C-6″), 165.14 (C-7′), 156.87 (C-9), 156.84 (C-2), 161.60 (C-5), 160.63 (C-4′), 133.66 (C-3), 131.53 (C-2′& C-6′), 121.22 (C-1′), 115.63 (C-3′& C-5′), 104.22 (C-10), 101.60 (C-1″), 99.33 (C-6), 94.25 (C-8), 76.65 (C-3″), 75.47 (c-5″), 73.96 (C-2″), 71.07 (C-4″).

2.3.4. Kaempfer-3-O-β-D-glucoside

^{1}H NMR (400 MHz, DMSO d_6) δ ppm 7.99 (d, J = 8.4 Hz, 2H), 6.83 (d, J = 8.4 Hz, 2H), 6.31 (d, J = 2 Hz, 1H), 6.10 (d, J = 2 Hz, 1H), 5.41 (d, J = 7.1 Hz, 1H). This compound was further confirmed using authentic compound.

2.3.5. HPLC-PDA-MS/MS

We used a Thermo Finigan LC system (Thermo electron Corporation, USA) coupled with an LCQ-Duo ion trap mass spectrometer with an ESI source (Thermo Quest) to analyze the extract. The C18 column (Zorbax Eclipse XDB-C18, Rapid resolution, 4.6 × 150 mm, 3.5 µm, Agilent, USA) was utilized. The mobile phase consisted of water and acetonitrile (ACN) (0.1% formic acid each) in which ACN was increased from 5% to 30% over 60 min in flow rate of 1 ml/ min and a 1:1 split before the ESI source. Thermo Quest auto sampler surveyor was used for samples injection. The software Xcalibur™ 2.0.7 (Thermo Scientific) used to control the instrument. The MS operated in the negative mode in a full scan (50–2000 m/z) (El Raey et al., 2019).

2.4. Molecular docking

The molecular docking analyses were done as detailed before (El-Hawary et al., 2020). In brief, the enzymes' structures were downloaded from protein data bank (www.pdb.org) with the corresponding bound ligands. The pdb codes were hyaluronidase (PDB id:1FCV), elastase (PDB id: 1Y93), collagenase (PDB id: 2D1N), Tyrosinase (PDB id: 2Y9X).

2.5. In vitro anti-aging activities

2.5.1. Total polyphenol content and DPPH assay

The total phenolic content was estimated by Folin Ciocalteu as detailed in (Ghareeb et al., 2018). Procedure of DPPH assay was handled according to (Clarke et al., 2013) and adapted to 96 well plate as described in (Ghareeb et al., 2018).

2.5.2. Enzyme inhibition assays

2.5.2.1. Anti- collagenase assay. Collagenase inhibition assay was performed according to (Kim et al., 2004) with minor modifications to be used in a microplate reader. The assay was carried out in 50 mM Tricine buffer (pH 7.5 with 400 mM NaCl and 10 mM $CaCl_2$). Collagenase enzyme obtained from *Clostridium histolyticum* (ChC – EC.3.4.23.3) was dissolved in the buffer and used at the initial concentration 0.8 units/mL as per the supplier's activity data. The synthetic substrate *N*-[3-(2-furyl) acryloyl] -Leu-Gly-Pro-Ala (FALGPA) was dissolved in the buffer to prepare a 2 mM solution. Samples (1000–7.81 µg/ mL) were incubated with the enzyme in the buffer for 15 min before the substrate is added to start the reaction. Absorbance at 490 nm was measured by the aid of microplate reader (TECAN, Inc.). The positive control used in this assay was EGCG and the percentage of collagenase inhibition (%) was calculated according to the formula: inhibition (%) = [1 − (s/c) × 100], where '**s**' is the corrected absorbance values of the collagenase inhibitor samples (the enzyme activity in presence of the samples), and '**c**' is the corrected absorbance values of the control samples (the enzyme activity in absence of the samples) (Elgamal, et al. 2021).

2.5.2.2. Anti-Elastase assay. Elastase inhibition assay was performed according to (Kim et al., 2004) with minor modifications. Briefly; Porcine pancreatic elastase enzyme was dissolved in sterile water to prepare a stock solution with a concentration of 3.33 mg/mL. N-Succinyl-Ala-Ala- Ala-*p*-nitroanilide (AAAPVN) was used as a substrate and dissolved in buffer to prepare a 1.6 mM solution, while EGCG was used as a positive control. The test substances were incubated for 15 min with the enzyme before adding the substrate to start the reaction. The final reaction mixture had 250 µL total volume and contained buffer, 0.8 mM AAAPVN, 1 µg/mL PE and 25 µg test substance. Samples (1000–7.81 µg/ mL) were incubated and absorbance values at 400 nm were measured in a 96 well plates using a Microplate reader (TECAN, Inc.). The percentage of elastase inhibition (%) was calculated according to the formula: inhibition (%) = [1 − (s/c) × 100],

Where '**s**' is the corrected absorbance of the samples containing elastase inhibitor (the enzyme activity in presence of the samples), and '**c**' is the corrected absorbance of controls (the enzyme activity in absence of the samples) (Elgamal, et al. 2021).

2.5.2.3. Anti-tyrosinase assay. Tyrosinase inhibition assay was performed using L-DOPA as substrate (Elgamal, et al. 2021). The reaction mixture (1000 µL) contained 15 µL of mushroom tyrosinase (2500 U mL^{-1}), 200 µL of samples, 100 µL of 5 mM L-DOPA, and 685 µL of phosphate buffer (0.05 M, pH 6.5). After adding L-DOPA, the reaction mixture was monitored at 475 nm for dopachrome formation using a Microplate reader (TECAN, Inc.). EGCG was used as a positive control. The samples concentration range in the assay was 1000–7.81 µg/ mL. Each measurement was made in triplicate. The percentage inhibition for this assay is calculated. The percentage of tyrosinase inhibition (%) was calculated according to the formula: inhibition (%) = [1 − (s/c) × 100], Where '**s**' is the corrected absorbance of the samples containing tyrosinase inhibitor (the enzyme activity in presence of the samples), and '**c**' is the corrected absorbance of controls (the enzyme activity in absence of the samples) (Batubara et al., 2010).

2.5.2.4. Anti-hyaluronidase assay. Hyaluronidase inhibition assay was performed according to Morgan-Elson fluorimetric method as in (Reissig et al., 1955) and modified by (Takahashi et al., 2003). Briefly, the reaction mixture was prepared in 2 ml-test tubes by adding 25 µL of calcium chloride (12.5 mM), 12.5 µL of each test sample (2.8 mg/ml) and hyaluronidase enzyme (1.5 mg/mL). The substrate hyaluronic acid (100 µL of 1 mg/ml in 0.1 M acetate buffer; pH 3.5) was used in the assay. The samples concentration range in the assay was 1000–7.81 µg/ mL. Then after, 25 µL of 0.8 M KBO_2 was added to all tubes that were placed in a water bath at 100 °C for 3 min. The tubes were then left to cool to ambient temperature and DMAB (800 µL, 4 g DMAB in 40 ml acetic acid and 5 ml 10 N HCl) was added. The tubes were incubated for 20 min and their content was transferred to respective wells in a 96-well plate. Fluorescence was detected using a Tecan Infinite microplate reader at 545 nm excitation and 612 nm emission (Elgamal, et al. 2021).

2.6. Statistical analysis

GraphPad Prism software (San Diego, CA. USA) was used to estimate the inhibitory concentration 50 (IC_{50}), the concentration required to inhibit 50% of enzyme under the assay conditions, from the graphic plots of the dose response curves. Statistical Package of the Social Sciences, SPSS version 23 (IBM SPSS software, USA) was used for data statistical analysis. The data were expressed as a mean ± SEM and analyzed using one-way analysis of variance.

3. Results and discussion

The phytochemical composition of *E. retusa* extract was investigated using HPLC-PDA-MS/MS which led to identification of 21 secondary metabolites. They included organic acids namely malic acid, cinnamoyl quinic acid derivatives, flavonols glycosides, coumarins and sulphated ellagic acid conjugates. Additionally, four secondary metabolites were isolated, and their identification was established based on UV, high resolution mass spectrometry, and ^{1}H & ^{13}C- NMR analyses. Kaempferol3-*O*-glucuronide and esculetin were isolated and identified for the first time from the plant, Table 1 and Fig. 1.

3.1. Molecular docking

Collagen and elastin are essential biomolecules in the extracellular matrix required to preserve the skin elasticity, flexibility, and strength. Overexpression of collagenase (MMP13) and elastase (MMP12) leads to the degradation of collagen and elastin, respectively. Some reports proved the stimulatory effect of elastase on other metalloproteinase enzymes, which leads to further acceleration of the matrix proteolytic degradation (Jabłońska-Trypuć et al., 2016). As wrinkles begin to form, elastase enzyme is secreted by fibroblasts, where it decreases the skin elasticity, and increases the elastic fibers tortuosity, which are the two early events in the wrinkle formation process (Tsuji et al., 2001). Hence, blocking the target enzymes collagenase and elastase would preserve skin elasticity and guard against skin aging.

Docking of *E. retusa* polyphenols showed that the compounds were able to fit properly inside the binding site and afforded lower binding free energy when compared to the reference polyphenol EGCG (Table 2). Compounds **10**, **8**, and **14** showed the best docking scores, which reflects minimum binding free energy of −20.10, −18.33, and −16.87 kcal/mol to collagenase enzyme, respectively versus −13.96 kcal/mol for EGCG. In terms of the interactions with the amino acid residues in the binding site, the compounds iterated some of the interactions afforded by the synthetic reference inhibitor, hydroxamic acid such as the Zn chelation, the hydrophobic interaction with His222 and Leu239, and the H-bonding interaction with Lue185. Moreover, the compounds showed to interact with Phe241 and Gly183, which are also afforded by the reference EGCG (Fig. 2).

It is noticeable that the common chemical feature in the scaffolds of the three compounds showing the best docking score is the glucuronide moiety that is ionized in the physiological pH acquiring a negatively charged carboxylate (COO–), which facilitates the Zn chelation in the collagenase's binding site. Other compounds lacking this moiety or those that were not able to afford this interaction with the zinc atom showed higher binding energy. This is evidenced upon comparing the docking scores and the binding site interactions afforded by quercetin 3-glucoside (has one ionized OH group) relative to kaempferol 3-glucoside (has no any ionized OH groups) (Table 2).

Interestingly, *E. retusa* polyphenols did not show the Zn chelation interaction upon docking them to the elastase enzyme, however they exhibited a well-fitting inside the binding site with a free binding energy ranged from −8.68 to −20.89 kcal/mol. Missing such an interaction would not likely diminish the elastase inhibitory activity of the compounds as it comes in agreement with a study by (Engel et al., 2005) who managed to design novel non-zinc binding metalloproteinase inhibitors. Compounds **13**, **5**, and **2** showed the minimum free binding energy and the best docking score of −20.89, −18.57, and −18.18 kcal/mol, respectively versus −27.02 kcal/mol for the polyphenol reference inhibitor EGCG. Compound **13**

Table 1 Chemical profiling of *E. retusa* aqueous methanolic extract.

No.	Proposed structure	UV	t_R	$[M-H]^-$	MS^2 (*m*/*z*)	References
1	Malic acid		1.34	133	115, 89	(Ghareeb et al., 2019)
2	*p*-Coumaroylquinic acid	280, 314	3.14	337	191, 173, 163	(Sobeh et al., 2017)
3	3-*O*-Feruloylquinic-acid	274, 304	3.58	367	193, 191, 173	(Sobeh et al., 2018)
4	5-*O*-Feruloylquinic acid	279, 310	4.89	367	193, 191, 173	(Jaiswal et al., 2010)
5	Kaempferol 3-*O*- glucuronide-7-*O*- glucoside[a]	266, 348	9.71	623	461, 447, 285	(Saleh, 1985)
6	Esculetin[b]		12.73	177	133, 89	
7	Quercetin 7-*O*- glucuronide	267, 372	14.32	477	301, 179	(Bergantin et al., 2017)
8	Quercetin 3-*O*- galacturonide	267, 356	14.97	477	301, 179	
9	Quercetin 3-*O*- glucuronide[b]	268, 355	15.38	477	301, 179	
10	Kaempferol 7-*O*- galacturonide	267, 355	16.70	461	285	
11	Kaempferol 7-*O*- glucuronide	267, 354	17.85	461	285, 151	(Bergantin et al., 2017)
12	Kaempferol *O*- glucuronide	267, 349	18.92	461	285	
13	Kaempferol 3-*O*- galacturonide	267, 349	20.17	461	285	
14	Kaempferol 3-*O*- glucuronide[b]	267, 348	21.10	461	285	
15	Kaempferol *O*- glucuronide	267, 348	22.49	461	285	
16	3,3′-di-*O*-methylellagic acid sulphate	272, 343	26.41	409	329	(Hussein, 2004)
17	Dimethoxy ellagic sulphate	270, 345sh	27.44	409	329	(Hussein, 2004)
18	Quercetin 3-*O*-glucoside[c]	267, 352	28.74	463	301, 179, 151	(Saleh, 1985)
19	Quercetin 3-*O*-pentoside	268, 351	30.49	433	301	(Sobeh et al., 2017)
20	Kaempferol 3-*O*-glucoside[b,c]	269, 349	32.95	447	285	(Sobeh et al., 2017)
21	3,3′,4-tri-*O*-methylellagic acid 4′-sulphate		33.99	423	343, 329	

[a] Previously reported from the plant (Saleh, 1985).
[b] isolated from the plant in the current study.
[c] isolated from the plant before (Ghareeb, T et al., 2018).

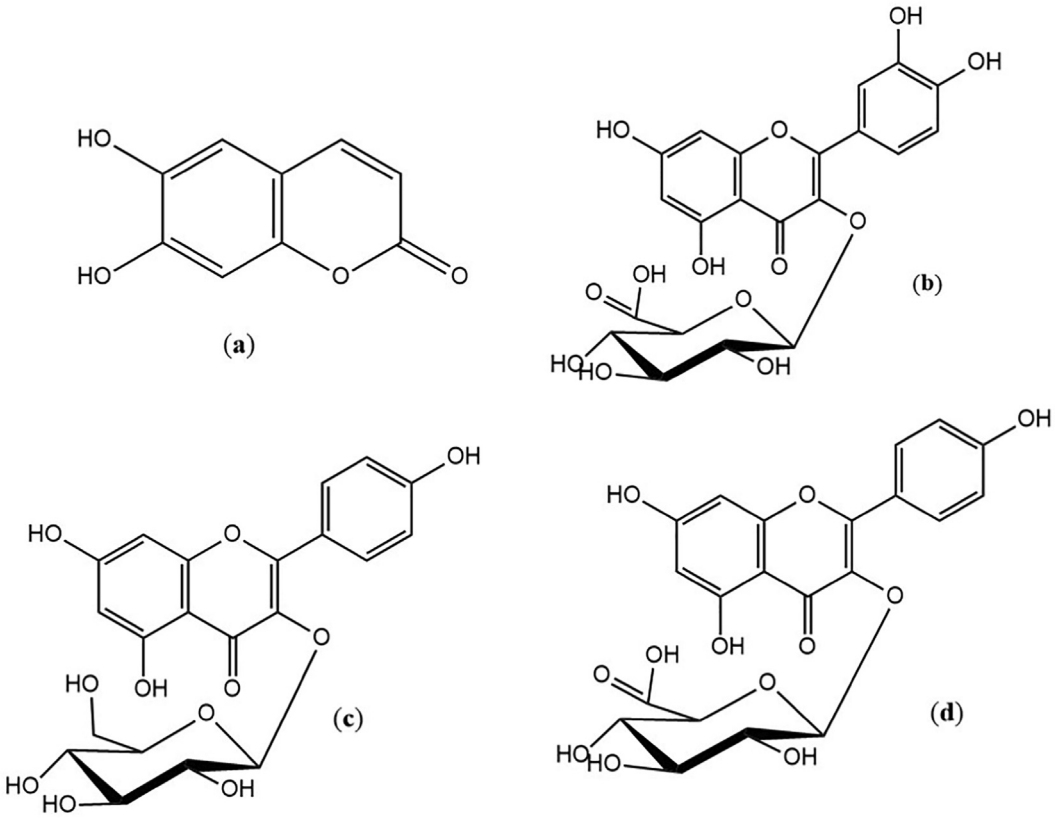

Fig. 1 Chemical structure of the isolated compounds from *E. retusa* extract. (a) Esculetin, (b) Quercetin -3-*O*-*β*-D-glucuronide, (c) Kaempferol -3-*O*-*β*-D-glucoside, (d) Kaempferol -3-*O*-*β*-D-glucuronide.

Table 2 Docking results (scoring functions and amino acids interactions) of the identified secondary metabolites from *E. retusa* and the reference compound EGCG on four enzymes (hyaluronidase, elastase, collagenase, and tyrosinase).

Compound (No.)	Hyaluronidase (1FCV)		Elastase (1Y93)		Collagenase (2D1N)		Tyrosinase (2Y9X)	
	Score (kcal/mol)	Interactions	Score (kcal/mol)	Interactions	Score (kcal/mol)	Interactions	Score (kcal/mol)	Interactions
Malic acid (**1**)	−10.97	Arg 244 (H bonding, ionic) Gln 271 (H bonding) Tyr 184 (H bonding)	−10.23	His 228 (H-bonding) His 222 (Ionic) His 183 (H-bonding through solvent) H_2O 326 (H-donner)	−10.41	Glu 223 (H bonding) Leu 185 (H bonding) Zn 270 (metal and ionic bonds)	−19.57	Asn 260 (H bonding) His 85 (Ionic bonds) Cu 400 (metal and ionic bonds) Cu 401 (metal and ionic bonds)
p-Coumaroylquinic acid (**2**)	−14.78	Glu 113 (H bonding) Gln 271 (H bonding) Tyr 184 (H bonding)	−18.18	His 222 (Ionic) His 183 (H-bonding through solvent) H_2O 326 (H-donner)	−13.36	Leu 185 (H bonding) Zn 270 (metal and ionic bonds) Pro 242 (H bonding) Ala 186 (H bonding) Tyr 244 (pi-H) Thr 245 (pi-H)	−15.24	Asn 260 (H bonding) His 85 (Ionic bonds) Met 280 (H bonding) Cu 400 (Ionic bonds) Cu 401 (Ionic bonds) His 263 (H-pi)
Esculetin (**3**)	−7.34	Glu 113 (H bonding)	−8.68	His 228 (pi-H)	−7.46	Glu 223 (H bonding) Val 219 (H bonding) His 222 (pi-pi)	−8.48	His 263 (pi-pi)
3-*O*-Feruloylquinic acid (**4**)	−15.67	Gln 271 (H bonding) Tyr 184 (H bonding) Arg 116 (H bonding, ionic)	−15.46	Pro 238 (H bonding through solvent) Leu 181 (H bonding through solvent) HOH 385 (H-donner)	−13.79	Phe 241 (H bonding) Leu 185 (H bonding) Zn 270 (metal and ionic bonds)	−15.33	Glu 322 (H bonding) His 85 (Ionic bonds) Cu 401 (metal and ionic bonds)
3,3′,4-tri-*O*-methylellagic acid 4′-sulfate (**5**)	−13.62	Gln 271 (H bonding)	−18.57	Lys 233 (H-bonding and ionic) Lys 241 (pi-H) Arg 249 (H bonding through solvent)	−12.95	Ala 188 (H bonding) Zn 270 (ionic bonds)	−16.85	His 85 (Ionic bonds) Glu 256 (H bonding) Cu 400 (metal and ionic bonds) Cu 401 (metal and ionic bonds)
3,3′-di-*O*-methylellagic acid sulfate (**6**)	−13.60	Gln 271 (H bonding)	−17.49	Thr 247 (H-bonding) H2O 479 (H-acceptor)	−15.03	Ala 188 (H bonding) Zn 270 (ionic bonds)	−18.86	His 85 (Ionic bonds) Cu 400 (metal and ionic bonds) Cu 401 (metal and ionic bonds)
Kaempferol-3-*O*-glucuronoside (**7**)	−13.45	Glu 113 (H bonding) Gln 271 (H bonding) Arg 116 (H bonding, ionic)	−12.33	Ala 184 (H-bonding through solvent) His 228 (pi-H) H_2O 472 (H-donner) H_2O 515 (H-donner)	−16.70	Leu 185 (H bonding) Zn 270 (metal and ionic bonds) Ala 186 (H bonding) Tyr 244 (pi-H)	−21.33	His 85 (Ionic bonds) Asn 260 (H bonding) Gly 281 (H bonding) Cu 400 (metal and ionic bonds) Cu 401 (metal and ionic bonds)

Table 2 (*continued*)

Compound (No.)	Hyaluronidase (1FCV)		Elastase (1Y93)		Collagenase (2D1N)		Tyrosinase (2Y9X)	
	Score (kcal/mol)	Interactions	Score (kcal/mol)	Interactions	Score (kcal/mol)	Interactions	Score (kcal/mol)	Interactions
Kaempferol 7-*O*-glucuronide (**8**)	−18.98	Glu 113 (H bonding) Tyr 55 (Hydrophobic)	−10.44	Thr 239 (H bonding through solvent) Pro 238 (H bonding through solvent)	−18.33	Leu 185 (H bonding) Zn 270 (metal and ionic bonds) Pro 242 (H bonding) Ala 186 (H bonding) Tyr 244 (pi-H) His 222 (pi-pi) Leu 239 (pi-H)	−19.00	His 85 (Ionic bonds) Val 248 (pi-H) Arg 268 (pi-cation) Cu 400 (metal and ionic bonds) Cu 401 (metal and ionic bonds)
kaempferol-3-glucoside (**9**)	−14.68	Gln 271 (H bonding)	−12.51	Lys 233 (H-bonding through solvent) Arg 249 (H-bonding through solvent) H2O 568 (H-acceptor)	−13.97	His 222 (pi-pi) His 232 (H-pi) Leu 185 (H bonding) Phe 241 (H bonding) Ala 186 (H bonding) Lue 185 (H bonding)	−13.07	Val 283 (H bonding) Arg 268 (H bonding) Met 257 (H bonding)
Kaempferol-3-*O*-glucuronide-7-*O*-glucoside (**10**)	−15.95	Glu 113 (H bonding) Tyr 55 (Hydrophobic)	−13.95	His 228 (H-bonding) Thr 239 (H bonding through solvent) H2O 398 (H-donner) H2O 472 (H-donner)	−20.10	Zn 270 (metal and ionic bonds) His 222 (pi-pi) Ala 186 (H bonding) Val 219 (H bonding) Thr 245 (H bonding)	−19.65	His 85 (Ionic bonds) Asn 260 (H bonding) Gly 281 (H bonding) Glu 322 (H bonding) His 263 (H-pi) Cu 400 (metal and ionic bonds) Cu 401 (metal and ionic bonds)
Quercetin-3-glucoside (**11**)	−16.68	Glu 113 (H bonding) Asp 111 (H bonding)	−16.14	Arg 249 (H-bonding through solvent) Lys 233 (H-bonding through solvent) Lys 241 (H-bonding and ionic) H2O 425 (pi-H)	−16.70	Zn 270 ((metal and ionic bonds) Ala 186 (H bonding) Leu 185 (H bonding)	−16.88	His 85 (Ionic bonds) Gly 281 (H bonding) Cu 400 (ionic bond) Cu 401 (ionic bond)
Quercetin 3-*O*-glucuronide (**12**)	−12.44	Tyr 55 (pi-H) Tyr 184 (H bonding) Trp 301 (pi-H)	−12.00	Arg 249 (H-bonding through solvent) Lys 233 (H-bonding and ionic) H2O 571 (H-donner) H2O 588 (H-donner)	−16.36	Zn 270 ((metal and ionic bonds) Ala 186 (H bonding) Leu 185 (H bonding)	−18.64	His 85 (hydrogen and ionic bonds) Asn 260 (H bonding) Cu 400 (ionic bond) Cu 401 (ionic bond)

(*continued on next page*)

Table 2 (*continued*)

Compound (No.)	Hyaluronidase (1FCV)		Elastase (1Y93)		Collagenase (2D1N)		Tyrosinase (2Y9X)	
	Score (kcal/mol)	Interactions	Score (kcal/mol)	Interactions	Score (kcal/mol)	Interactions	Score (kcal/mol)	Interactions
Quercetin-3-*O*-pentoside (**13**)	−14.53	Glu 113 (H bonding) Tyr 55 (Hydrophobic) Ser 303 (Hydrophobic) Ser 304 (Hydrophobic)	−20.89	Ala 182 (H-bonding) H_2O 402 (H-acceptor)	−12.66	Glu 223 (H bonding) His 222 (H-pi) Gly 183 (H bonding)	−8.20	His 85 (H bonding) Asn 81 (H bonding) Glu 322 (H bonding)
Quercetin 7-*O*-D-glucuronide (**14**)	−16.15	Glu 113 (H bonding) Tyr 55 (Hydrophobic Arg 116 (H bonding, ionic) Arg 274 (H bonding)	−15.27	His 228 (pi-H) H_2O 528 (H-acceptor)	−16.87	Zn 270 (metal bond) Pro 242 (H bonding) Tyr 244 (H bonding through solvent) Gly 183 (H bonding through solvent)	−19.06	His 85 (Ionic bonds) Ala 246 (H bonding) Cu 400 (ionic bonds) Cu 401 (metal and ionic bonds)
EGCG (**15**)	−17.97	Glu 113 (two H bonding) Ser 303 (H bonding)	− 27.02	His 228 (pi-H) Tyr 240 (H-bonding through solvent) H_2O 511 (H-donner)	−13.96	Phe 241 (H bonding) Ile 243 (H bonding) Leu 218 (H bonding) Gly 183 (H bonding)	−14.12	Glu 322 (H bonding) His 85 (pi-H)

was the only polyphenol able to afford H-bonding interaction with Ala182 residue afforded by the reported synthetic inhibitor hydroxamic acid (Table 2, Fig. 3).

Melanin production in melanocytes is under the control of the key enzyme tyrosinase (polyphenol oxidase), which first mediates the hydroxylation of tyrosine to DOPA (3, 4-dihydroxyphenylalanine) followed by oxidation of DOPA into DOPAquinone. Hyperpigmentation due to overproduction of melanin is very well related to skin aging and is enhanced by many internal factors such as age-related disturbances in hormones levels and external factors such as excessive exposure to UV radiation, deleterious pollutants, chemicals, and some drugs, thus tyrosinase inhibitors can improve skin appearance and lightening and help slowdown skin aging (Bae-Harboe and Park, 2012).

The crystal structure of tyrosinase revealed that it is a metalloenzyme containing two tetragonal copper ions in its binding site. It was reported that Asn 260, His 263, and Met 280 are important residues for the interactions with tyrosinase inhibitors as well as the metal chelation capability (Moulishankar and Lakshmanan, 2020). Polyphenols identified in the studied extracts showed to be properly fitted in the binding site of tyrosinase with minimum free binding energy as low as −21.33 kcal/mol, which was the best docking score achieved

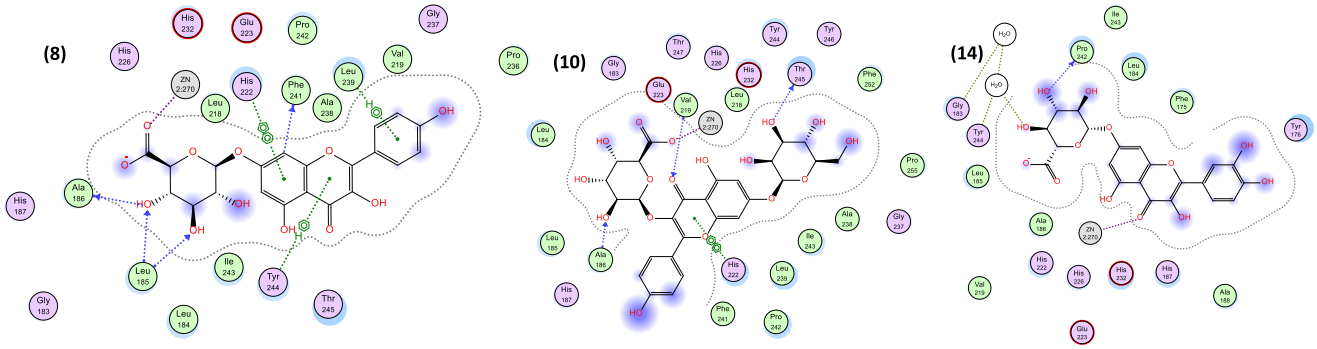

Fig. 2 2D-interactions of compounds, (8) Kaempferol 7-*O*-glucuronide, (10) Kaempferol 3-*O*-glucuronide-7-*O*-glucoside, (14) Quercetin 7-*O*-glucuronide with amino acid residues on collagenase. Numbers are from Table 2.

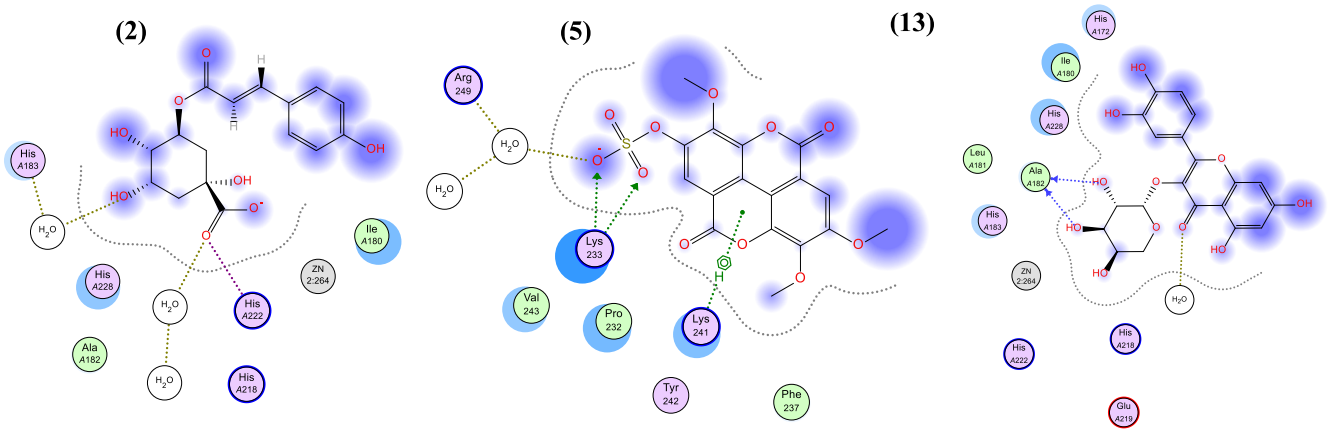

Fig. 3 2D-interactions of compounds, (2) *p*-Coumaroylquinic acid, (5) 3,3′,4-tri-*O*-methylellagic acid 4′-sulfate and (13) Quercetin 3-*O*-pentoside with amino acid residues on elastase. Numbers are from Table 2.

by compound **7**. Compounds **10** and **1** showed as well much lower free binding energy of −19.65 and −19.57 kcal/mol, respectively compared to other docked compounds and the reference EGCG (Table 2). In their ionized state at the physiological pH, the three compounds were characterized by having a negative charge on the carboxylate group of maleic acid (compound **1**) or the glucuronide moiety of kaempferol 3-glucuronide (compound **7**) and kaempferol 3-glucuronide-7-glucoside (compound **10**), thus, they were able to chelate the Cu ions in the binding site, which is a very crucial interaction in tyrosinase inhibitors. Such as interaction was also afforded by all the negatively charged compounds that showed better free binding energy relative to the unionized compounds and the unionized form of EGCG. Moreover, these three compounds were able to show at least one of the two interactions with Asn260 or His263, which were regarded as important interactions of tyrosinase inhibitors (Fig. 4). Our results come in agreement with the study by (Cabanes et al., 1994) that reported the potential of kojic acid to block the tyrosinase enzyme by virtue of copper chelation.

Hyaluronic acid is a glycosaminoglycan derivative and represents one of the major and essential components in the skin extracellular matrix, where it facilitates the transportation of nutrients and waste products through it and maintains the skin elasticity and moisture. It plays an important role as well in the tissues renewal, remodeling, and repair. Hyaluronidase is a member of the hyaluronoglucosidase enzymes family that catalyzes the cleavage of hyaluronic acid at the links binding the N-acetylglucosamine and glucoronate units. The crystal structure of the ligand-protein complex of hyaluronidase enzyme isolated from the bee venom (shares 30% sequence identity with the human isoform) showed some important interactions with the residues Tyr 55, Glu 113, Tyr 184, among others (Marković-Housley et al., 2000).

Our *in silico* results showed that the polyphenols identified in the *E. retusa* extract showed a free binding energy range of −7.34 to −18.98 kcal/mol upon docking into hyaluronidase binding site and were able to iterate some of the reported interactions with the co-crystallized ligand. Compounds **8**, **11**, and **14** showed the best docking scores and minimum binding free energy of −18.98, −16.68, and −16.15 kcal/mol, respectively (Table 2). They afforded the reported H-bonding interaction with Glu113 and the hydrophobic (pi-H) interaction with Tyr55 residues. Moreover, they showed some additional polar

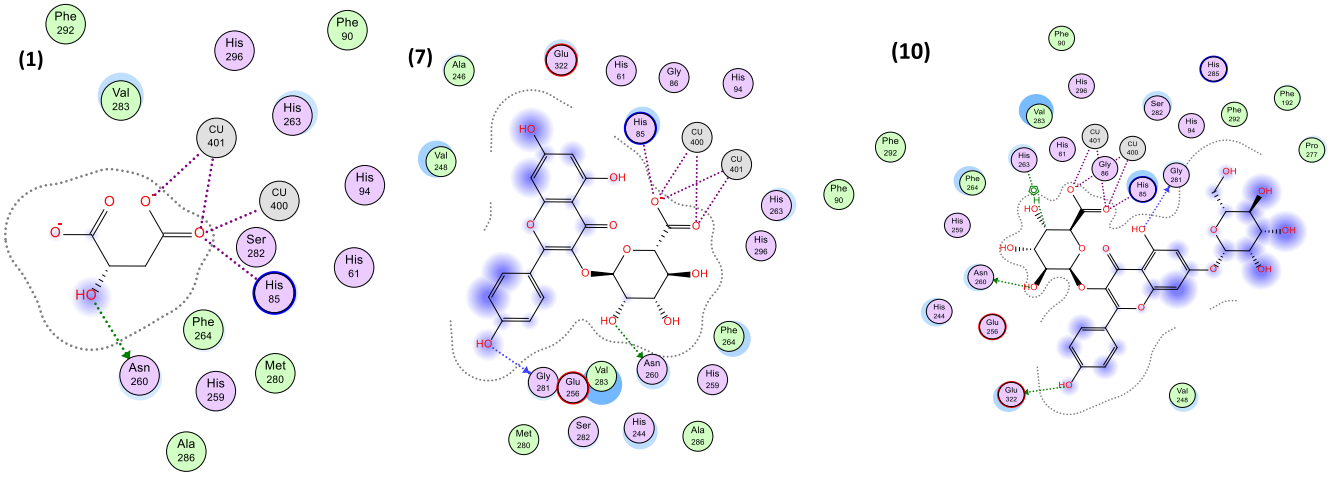

Fig. 4 2D-interactions of compounds, (1) Malic acid, (7) Kaempferol 3-*O*-glucuronide and (10) Kaempferol 3-*O*-glucuronide 7-*O*-glucoside with amino acid residues on tyrosinase. Numbers are from Table 2.

interactions with other amino acids in the binding site such as Asp111 (compound **11**), Arg116, Arg274 (compound **14**) as illustrated in (Fig. 5).

A general overview at our *in silico* study can lead to conclude that the polyphenols identified in the studied extract showed to be well accommodated in the binding sites of the four target enzymes with appreciable free binding energy of −16 kcal/mol on average. Out of the docked polyphenols, three, five, six, and nine compounds showed better free binding energy than the average (−16 kcal/mol) towards the enzymes hyaluronidase, elastase, collagenase, and tyrosinase, respectively. This could suggest that tyrosinase enzyme is the most prominent target enzyme for this group of polyphenols. Moreover, we can conclude that compounds **8**, **10**, and **14** are the most effective as they showed the minimum free binding energy towards at least two out of the four enzyme targets used in this study (Table 2).

3.2. *In vitro* anti-aging activities

3.2.1. *Antioxidant activity and enzyme inhibition assays*

Our skin is at a relatively higher incidence of generating metabolic reactive oxygen species (ROS) such as hydroxyl radicals, superoxide anions, and single oxygen because of direct exposure to ionizing radiation, chemical and mechanical insults, environmental pollutants and other deleterious causing factors. Reports show that UV radiation contributes to almost 80% to generate ROS in skin, which in turn would lead to developing a state of oxidative stress in case natural body defense mechanisms failed to hinder the excessive generation of ROS [27]. Oxidative stress promotes skin aging and damage via several mechanisms including DNA damage, activation of JAK/STAT, NF-kB, and MAPK/AP-1 signaling pathways, stimulating autophagy and apoptosis pathways, inducing autoimmune responses against keratinocytes and melanocytes. Endogenous skin defense strategies engage a huge family of antioxidant enzymes including superoxide dismutase, catalase, and glutathione peroxidase that neutralize the different ROS (Reuter et al., 2010). However, ingestion of dietary antioxidants from different food and plant sources plays a crucial role in fighting off ROS and keeping healthy young-looking skin. In DPPH assay, the studied E. retusa extract demonstrated considerable antioxidant activity (IC_{50} μg/mL = 11.32) compared to the reference polyphenol EGCG (IC_{50} μg/mL = 3.3 1). This is most likely due to its high total phenolic content evaluated to be 255 mg GAE/g extract. Such an action would augment the anti-aging properties of the extract and point out the value of using the extract in different anti-aging cosmetic applications.

Results from the *in silico* study showed a promising potential for E. retusa extract to interfere with some of the prominent enzyme targets involved in the development of skin aging signs. Thus, the total plant extract along with four purely isolated compounds; namely kaempferol 3-O-glucoside (**9**), kaempferol 3-O-glucuronide (**7**), quercetin 3-O-glucuronide (**12**), and esculetin (**3**) were evaluated to block these target enzymes using *in vitro* inhibitory assays. As shown in (Table 3), the extract and the four isolated compounds showed comparable IC_{50} values against the four enzymes relative to the reference EGCG. As revealed by the molecular docking, E. retusa extract was most active against tyrosinase enzyme with of IC_{50} of 39.5 μg/mL and least active against hyaluronidase enzyme with IC_{50} of 49.1 μg/mL. The four individual compounds showed the same activity pattern again as they were most active against tyrosinase, least active against hyaluronidase, and with moderate activity against collagenase and elastase enzymes, which comes in accordance with the results of the *in silico* study (Table 3).

Esculetin showed the weakest activity against all the four target enzymes as it exhibited the highest IC_{50} values, which comes in agreement with the results of the molecular docking as it showed the highest free binding energy ever relative to the rest of compounds (Tables 2 and 3). Regarding the inhibitory activities of the other three compounds against elastase and hyaluronidase enzymes, compound **9** was the most active followed by compound **7**, and finally compound **12** with IC_{50} of 55.53, 60.77, and 66.27 μM, respectively against elastase and 58.21, 65.31, and 77.76 μM, respectively against hyaluronidase enzyme. This comes in match with the free binding energy values obtained from the molecular docking study (Tables 2 and 3).

As for the collagenase and tyrosinase inhibitory activities, the same previous pattern was obtained again, where compound **9** showed to be the most active followed by **7**, and finally **12** (Table 3). However, this activity pattern was not in match with the *in silico* study results that revealed that compound **7** showed the minimum free binding energy followed by **12** and finally **9** towards both collagenase and tyrosinase

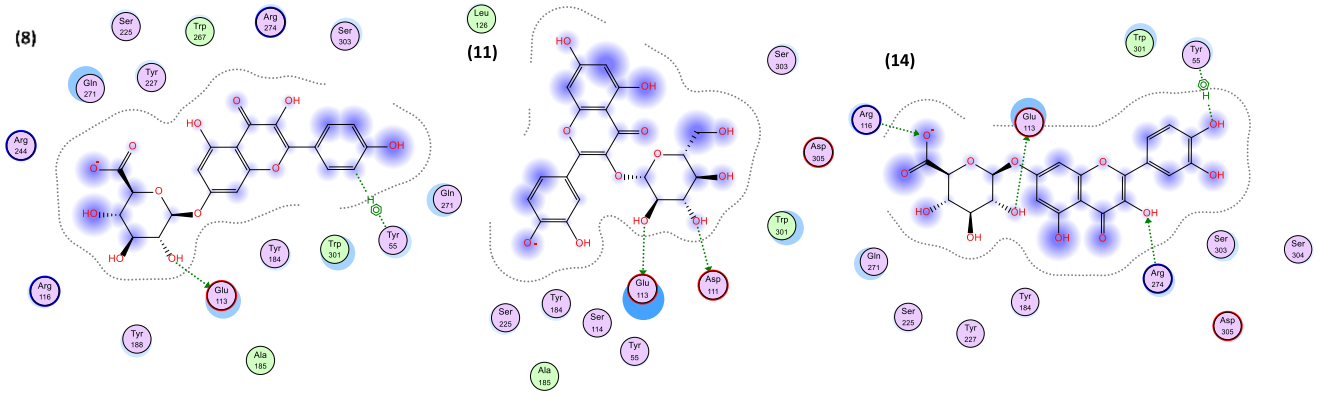

Fig. 5 2D-interactions of compounds (8) Kaempferol 7-*O*-glucuronide, (11) Quercetin 3-*O*-glucoside and (14) Quercetin 7-*O*-glucuronide with amino acid residues on hyaluronidase. Numbers are from Table 2.

Table 3 Enzyme inhibitory activities against collagenase, elastase, hyaluronidase and tyrosinase enzymes. Numbers are from Table 2. Compounds are arranged according to their activities.

Sample	Collagenase	Elastase	Hyaluronidase	Tyrosinase
	IC_{50} µg, mean ± SEM, n = 3			
Total extract	45.7 ± 1.2	39.6 ± 0.85	49.1 ± 0.88	39.5 ± 1.1
Compounds	IC_{50} µM, mean ± SEM, n = 3			
Esculetin* (**3**)	220.05 ± 6.74	180.76 ± 5.33	225.67 ± 5.33	169.53 ± 7.86
Quercetin-3-*O*-glucuronide* (**12**)	66.27 ± 2.51	53.72 ± 1.90	77.76 ± 1.36	53.93 ± 6.49
Kaempferol −3-*O*-glucuronide* (**7**)	60.77 ± 2.01	52.34 ± 2.16	65.31 ± 3.68	39.145 ± 3.68
Kaempferol −3-*O*-glucoside* (**9**)	55.53 ± 2.9	43.49 ± 2.19	58.21 ± 3.35	35.46 ± 1.67
EGCG* (reference compound)	52.14 ± 2.83	37.35 ± 3.06	52.58 ± 2.4	31.2 ± 1.99

* The *in vitro* results are in accordance with *in silico* results.

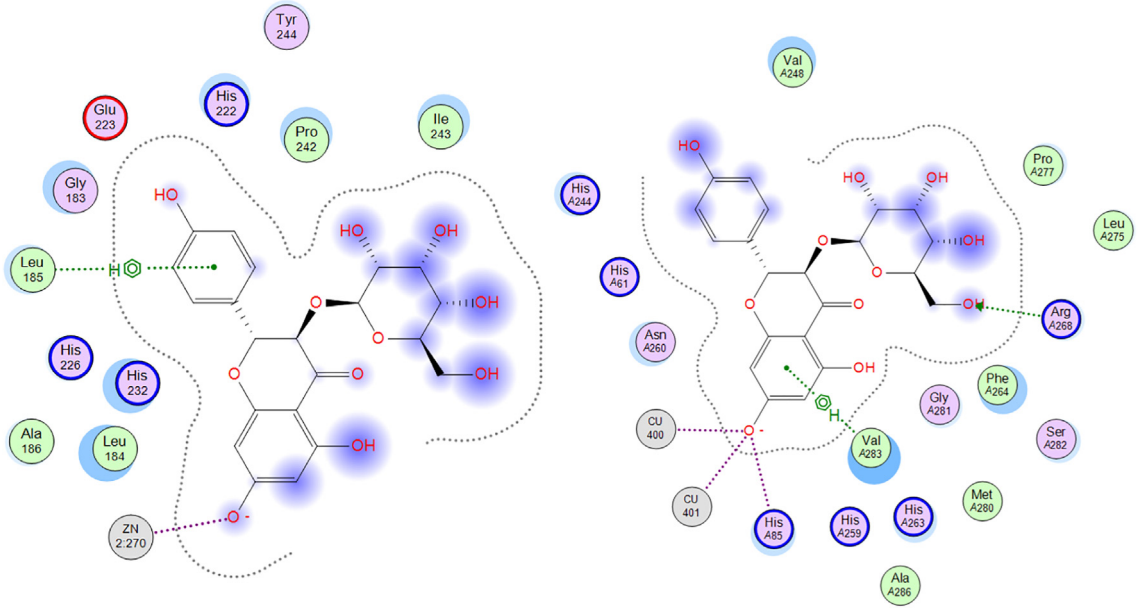

Fig. 6 2D-interactions of kaempferol 3-O-glucoside with amino acid residues in collagenase (left) and tyrosinase (right) active sites.

enzyme (Table 2). Exploring the chemical scaffold of these three compounds shows that compounds **7** and **12** are negatively charged at the physiological pH, whereas the ionized form of **9** does not seem to be predominant at the same pH. Thus, compound **9** was not able to afford the important metal chelation interaction with the zinc and copper ions upon docking into the binding sites of collagenase and tyrosinase enzymes, respectively (Table 2). The same enzyme inhibitory activity and free binding energy patterns were obtained by the reference EGCG on both collagenase and tyrosinase enzymes. Thus, we decided to use the forced ionization tool on MOE software to dock the ionized form of kaempferol 3-O-glucoside (**9**) and EGCG. Interestingly, compared to the unionized parent compounds, the ionized forms of **9** and EGCG showed much better free binding energy of −16.36 and −18.50 kcal/mol, respectively towards collagenase enzyme, and −21.80 and −19.50 kcal/mol, respectively towards tyrosinase enzyme. They afforded the important reported metal chelation interactions among other polar and nonpolar interactions with the amino acid residues in the binding sites of both enzymes (Fig. 6). Thus, we can conclude that the inhibitory activity of kaempferol 3-O-glucoside (**9**) and EGCG towards collagenase and tyrosinase enzymes depends, largely, on their ionized forms.

4. Conclusions

The phytochemical investigation of the aerial parts extract from *E. retusa* led to identifying 21 secondary metabolites, most of them are polyphenol derivatives and isolation of four secondary metabolites. The extract and four isolated compounds showed appreciable inhibitory activity against collagenase, elastase, hyaluronidase, and tyrosinase enzymes, which are significantly engaged in skin aging prognosis. The extract as well showed substantial antioxidant potential and its compounds afforded stable complexes with the aforementioned enzymes showing minimum free binding energy in the molecular docking. This wide range of activities could be attributed to the high content of polyphenolics in the extract. Based on two

thorough *in silico* and *in vitro* studies accomplished in the course of this work, we can conclude that *E. retusa* extract could be considered as a potential candidate, for further evaluation as a remedy for delaying and fighting off skin aging and its associated signs.

Declaration of Competing Interest

The authors declare no conflict of interest.

Acknowledgments

The authors would like to thank Prof. Ibrahim El-Garf, Prof. of Plant Taxonomy, Faculty of Science, Cairo University for identifying the plant and Dr. R. Rashied for collecting the docking data. The authors would like to thank Prof. Wink for giving us the opportunity to collect LC-MS data at his lab.

References

Altyar, A.E., Ashour, M.L., Youssef, F.S., 2020. *Premna odorata*: Seasonal metabolic variation in the essential oil composition of its leaf and verification of its anti-ageing potential via in vitro assays and molecular modelling. Biomolecules 10, 879.

Anusuya, N., Raju, K., Manian, S., 2010. Hepatoprotective and toxicological assessment of an ethnomedicinal plant Euphorbia fusiformis Buch.-Ham. ex D. Don. J. Ethnopharmacol. 127, 463–467.

Bae-Harboe, Y.-S.C., Park, H.-Y., 2012. Tyrosinase: a central regulatory protein for cutaneous pigmentation. J, Invest. Dermatol. 132, 2678–2680.

Bakr, R.O., El-Raey, M.A.E.-A., Farouk, C.N., Ahmed, H.E., El-Said, O.M., 2012. Radical scavenging activity and cytotoxicity of *Euphorbia hirta* l. Int. J. Phytomed. 4, 525.

Batubara, I., Darusman, L.K., Mitsunaga, T., Rahminiwati, M., Djauhari, E., 2010. Potency of Indonesian medicinal plants as tyrosinase inhibitor and antioxidant agent. J. Biol. Sci. 10, 138–144.

Bergantin, C., Maietti, A., Cavazzini, A., Pasti, L., Tedeschi, P., Brandolini, V., Marchetti, N., 2017. Bioaccessibility and HPLC-MS/MS chemical characterization of phenolic antioxidants in Red Chicory (*Cichorium intybus*). J. Funct. Foods 33, 94–102.

Cabanes, J., Chazarra, S., Garcia-Carmona, F., 1994. Kojic acid, a cosmetic skin whitening agent, is a slow-binding inhibitor of catecholase activity of tyrosinase. J. Pharm. Pharmacol. 46, 982–985.

Clarke, G., Ting, K.N., Wiart, C., Fry, J., 2013. High correlation of 2, 2-diphenyl-1-picrylhydrazyl (DPPH) radical scavenging, ferric reducing activity potential and total phenolics content indicates redundancy in use of all three assays to screen for antioxidant activity of extracts of plants from the Malaysian rainforest. Antioxidants 2, 1–10.

Elgamal, A.M., Ahmed, R.F., Abd-ElGawad, A.M., El Gendy, A.E., Elshamy, A.I., Nassar, M.I., 2021. Chemical profiles, anticancer, and anti-aging activities of essential oils of *Pluchea dioscoridis* (L.) DC. and *Erigeron bonariensis* L. Plants. 10 (667).

El Raey, M.A., El-Hagrassi, A.M., Osman, A.F., Darwish, K.M., Emam, M., 2019. Acalypha wilkesiana flowers: Phenolic profiling, cytotoxic activity of their biosynthesized silver nanoparticles and molecular docking study for its constituents as Topoisomerase-I inhibitors. Biocataly. Agric. Biotechnol. 20, 101243.

El-Hawary, S.S., Sobeh, M., Badr, W.K., Abdelfattah, M.A.O., Ali, Z. Y., El-Tantawy, M.E., Rabeh, M.A., Wink, M., 2020. HPLC-PDA-MS/MS profiling of secondary metabolites from *Opuntia ficus-indica* cladode, peel and fruit pulp extracts and their antioxidant, neuroprotective effect in rats with aluminum chloride induced neurotoxicity. Saudi J. Biol. Sci. 27, 2829–2838. https://doi.org/10.1016/j.sjbs.2020.07.003.

Engel, C.K., Pirard, B., Schimanski, S., Kirsch, R., Habermann, J., Klingler, O., Schlotte, V., Weithmann, K.U., Wendt, K.U., 2005. Structural basis for the highly selective inhibition of MMP-13. Chem. Biol. 12, 181–189.

Eun Lee, K., Bharadwaj, S., Yadava, U., Gu Kang, S., 2019. Evaluation of caffeine as inhibitor against collagenase, elastase and tyrosinase using *in silico* and *in vitro* approach. J. Enzyme Inhibit. Med. Chem. 34, 927–936.

Ghareeb, M.A., Mohamed, T., Saad, A.M., Refahy, L.A.-G., Sobeh, M., Wink, M., 2018. HPLC-DAD-ESI-MS/MS analysis of fruits from *Firmiana simplex* (L.) and evaluation of their antioxidant and antigenotoxic properties. J. Pharm. Pharmacol. 70, 133–142.

Ghareeb, M.A., Sobeh, M., El-Maadawy, W.H., Mohammed, H.Sh., Khalil, H., Botros, S., Wink, M., 2019. Chemical profiling of polyphenolics in *Eucalyptus globulus* and evaluation of its hepato–renal protective potential against cyclophosphamide induced toxicity in mice. Antioxidants 8, 415. https://doi.org/10.3390/antiox8090415.

Ghareeb, T., El-Toumy, S., Elgendy, H., Haggag, E., 2018. Secondary metabolites and hepatoprotective activity of *Euphorbia retusa*. J. Adv. Pharm. Res. 2, 283–291.

Haba, H., Lavaud, C., Magid, A.A., Benkhaled, M., 2009. Diterpenoids and triterpenoids from *Euphorbia retusa*. J. Nat. Prod. 72, 1258–1264.

Hussein, S.A.M., 2004. Phenolic sodium sulphates of *Frankenia laevis* L. Die Pharmazie – Int. J. Pharm. Sci. 59, 304–308.

Jabłońska-Trypuć, A., Matejczyk, M., Rosochacki, S., 2016. Matrix metalloproteinases (MMPs), the main extracellular matrix (ECM) enzymes in collagen degradation, as a target for anticancer drugs. J. Enzyme Inhibit. Med. Chem. 31, 177–183.

Jaiswal, R., Patras, M.A., Eravuchira, P.J., Kuhnert, N., 2010. Profile and characterization of the chlorogenic acids in green Robusta coffee beans by LC-MS n: Identification of seven new classes of compounds. J. Agric. Food. Chem. 58, 8722–8737.

Kim, Y.-J., Uyama, H., Kobayashi, S., 2004. Inhibition effects of (+)-catechin–aldehyde polycondensates on proteinases causing proteolytic degradation of extracellular matrix. Biochem. Biophys. Res. Commun. 320, 256–261.

Kumarappan, C.T., Jaswanth, S., Subhash, C.M., 2011. Hepatoprotective effect of *Euphorbia hirta* on carbon tetrachloride induced liver injury in rats. J. Pharm. Allied Sci. 8.

Lee, S., Yu, J.S., Phung, H.M., Lee, J.G., Kim, K.H., Kang, K.S., 2020. Potential anti-skin aging effect of (-)-catechin isolated from the root bark of *Ulmus davidiana* var. japonica in tumor necrosis factor-α-stimulated normal human dermal fibroblasts. Antioxidants 9, 981.

Marković-Housley, Z., Miglierini, G., Soldatova, L., Rizkallah, P.J., Müller, U., Schirmer, T., 2000. Crystal structure of hyaluronidase, a major allergen of bee venom. Structure 8, 1025–1035.

Matos, M.S., Romero-Díez, R., Álvarez, A., Bronze, M.R., Rodríguez-Rojo, S., Mato, R.B., Cocero, M.J., Matias, A.A., 2019. Polyphenol-rich extracts obtained from winemaking waste streams as natural ingredients with cosmeceutical potential. Antioxidants 8, 355.

Moulishankar, A., Lakshmanan, K., 2020. Data on molecular docking of naturally occurring flavonoids with biologically important targets. Data in brief 29, 105243.

Osman, S.M., El-Haddad, A.E., El-Raey, M.A., Abd El-Khalik, S.M., Koheil, M.A., Wink, M., 2016. A new octadecenoic acid derivative from *Caesalpinia gilliesii* flowers with potent hepatoprotective activity. Pharm. Magazine 12, S332.

Reissig, J.L., Strominger, J.L., Leloir, L.F., 1955. A modified colorimetric method for the estimation of N-acetylamino sugars. J. Biol. Chem. 217, 959–966.

Reuter, S., Gupta, S.C., Chaturvedi, M.M., Aggarwal, B.B., 2010. Oxidative stress, inflammation, and cancer: how are they linked?. Free Radical Biol. Med. 49, 1603–1616.

Saleem, H., Zengin, G., Locatelli, M., Mollica, A., Ahmad, I., Mahomoodally, F.M., Abidin, S.A.Z., Ahemad, N., 2019. In vitro biological propensities and chemical profiling of *Euphorbia milii* Des Moul (Euphorbiaceae): A novel source for bioactive agents. Ind. Crops Prod. 130, 9–15.

Saleh, N.A., 1985. Flavonol glycosides of E*uphorbia retusa* and *E. sanctae*-catharinae. Phytochemistry 24, 371–372.

Sdayria, J., Rjeibi, I., Feriani, A., Ncib, S., Bouguerra, W., Hfaiedh, N., Elfeki, A., Allagui, M.S., 2018. Chemical composition and antioxidant, analgesic, and anti-inflammatory effects of methanolic extract of Euphorbia retusa in mice. Pain Res. Manage.

Shaaban, M., Ali, M., Tala, M.F., Hamed, A., Hassan, A.Z., 2018. Ecological and phytochemical studies on Euphorbia retusa (Forssk.) from Egyptian habitat. J. Analy. Methods Chem.

Sobeh, M., Hassan, S.A., El Raey, M.A., Khalil, W.A., Hassan, M.A., Wink, M., 2017. Polyphenolics from *Albizia harveyi* exhibit antioxidant activities and counteract oxidative damage and ultrastructural changes of cryopreserved bull semen. Molecules 22, 1993.

Sobeh, M., Mahmoud, M.F., Petruk, G., Rezq, S., Ashour, M.L., Youssef, F.S., El-Shazly, A.M., Monti, D.M., Abdel-Naim, A.B., Wink, M., 2018. *Syzygium aqueum*: A polyphenol-rich leaf extract exhibits antioxidant, hepatoprotective, pain-killing and anti-inflammatory activities in animal models. Front. Pharmacol. 9, 566.

Takahashi, T., Ikegami-Kawai, M., Okuda, R., Suzuki, K., 2003. A fluorimetric Morgan-Elson assay method for hyaluronidase activity. Anal. Biochem. 322, 257–263.

Tsuji, N., Moriwaki, S., Suzuki, Y., Takema, Y., Imokawa, G., 2001. The role of elastases secreted by fibroblasts in wrinkle formation: implication through selective inhibition of elastase activity. Photochem. Photobiol. 74, 283–290.